ROYAL SOCIETY OF CHEMISTRY

Check for updates

White light emission in low-dimensional perovskites

Daniele Cortecchia, [ID] *[ab] Jun Yin,[c] Annamaria Petrozza [ID] [b] and Cesare Soci*[ad]

Low-dimensional perovskites are rapidly emerging due to their distinctive emission properties, consisting of ultrabroad and highly Stokes shifted luminescence with pure white light chromaticity, which makes them very attractive for solution-processed light-emitting devices and scintillators. To foster the design of new materials and their device applications, it is timely to review the relation between perovskite structural properties and the photophysical phenomena underlying their unique light emission characteristics. From a number of recent studies, it has emerged that broadband emission properties in metal halide frameworks are very common, stemming from the self-localization of small polaron species at specific sites of the inorganic lattice, with a wide energy distribution. This review aims to provide an account of the current understanding of the photophysical processes underpinning luminescence broadening and highly efficient emission in various classes of low-dimensional metal-halide frameworks, and to highlight their potential for solution-processed optoelectronic device applications. The discussion will additionally establish a wider perspective on the role of intrinsic and extrinsic self-trapping, formation of polarons and their effect on charge generation and transport in low-dimensional perovskites.

1 Introduction

Three-dimensional (3D) hybrid perovskites have rapidly established new paradigms for solution processed photovoltaics (reaching power conversion efficiencies up to 22%)[1] and light emitting devices.[2,3] At an equally fast pace, low-dimensional perovskites are opening new frontiers for solution-processable optoelectronic devices.[4,5] Primarily based on self-assembled metal–organic frameworks with highly tunable composition and reduced dimensionality (2D, 1D or 0D), this class of materials adds synthetic versatility to the standard 3D perovskite structure, providing distinctive advantages for light-emitting applications achievable by structural design:[6] strong exciton localization effects result in an unusually large Stokes shift,[7] which reduces the luminescence self-absorption and thermal quenching; an ultrabroad luminescence spectral width yields purely white chromaticity from a single emissive material;[8] the hydrophobicity of the templating organic cations significantly improves the material stability in ambient conditions;[9] and,

furthermore, the presence of heavy ions provides a large absorption cross section for ionizing radiation.[10] These features make low-dimensional perovskites particularly appealing for white light emitting devices (diodes, transistors and lasers) and large area X-ray scintillators for solid-state lighting, display, medical, and security applications. Recent progress in the synthesis of new classes of low-dimensional perovskites has revealed widespread broadband emissive characteristics. In these systems, the ability to govern the optoelectronic properties through rational synthetic design is conditional on the deep understanding of their unusual photophysical properties. This review aims at consolidating the recent understanding of the processes underpinning luminescence broadening and highly efficient emission in a variety of low-dimensional hybrid perovskites, with foreseeable device applications. Specifically, experimental and theoretical studies highlighted the role of charge self-trapping in the emission characteristics of low-dimensional perovskites, implicating the ultrafast formation of emissive color centers at specific inorganic lattice sites. From a broader fundamental standpoint, a unified picture of (small) polaron formation in relation to structural and compositional properties provides common ground to discuss implications for charge generation and transport in metal halide frameworks with different dimensionalities, beyond their luminescence characteristics.

1.1 From 3D to low dimensional perovskites

Three dimensional (3D) perovskites have the general formula AMX_3, where $X = F^-$, Cl^-, Br^-, I^-, B is a divalent cation

[a] *Energy Research Institute@NTU (ERI@N), Interdisciplinary Graduate School, Nanyang Technological University, 50 Nanyang Drive, 637553, Singapore. E-mail: csoci@ntu.edu.sg*

[b] *Istituto Italiano di Tecnologia, Centre for Nano Science and Technology (CNST@PoliMi), Milan, 20133, Italy. E-mail: daniele.cortecchia@iit.it*

[c] *Division of Physical Science and Engineering, King Abdullah University of Science and Technology, Thuwal 23955-6900, Saudi Arabia*

[d] *Division of Physics and Applied Physics, School of Physical and Mathematical Sciences, Nanyang Technological University, 21 Nanyang Link, 637371, Singapore*

4956 | *J. Mater. Chem. C*, 2019, 7, 4956–4969

This journal is © The Royal Society of Chemistry 2019

(*e.g.* Sn^{2+}, Pb^{2+}) and A is a monovalent metal or organic cation.[11] This structure is characterized by a continuous 3D network of corner-sharing MX_6 octahedra, while A is 12-fold coordinated in the cuboctahedral cavities, which limit the size of the cation to be enclosed.[12] The Goldschmidt tolerance factor $t = (R_A + R_X)/\sqrt{2}(R_M + R_X)$ and the octahedral factor $\mu = R_M/R_X$ (R_A, R_M and R_X are the effective ionic radii of the corresponding ions) help to predict whether A^+ would fit in the 3D perovskite structure, which is stable when $0.8 < t < 1$ and $0.442 < \mu < 0.895$.[13,14] Big cations disrupt the 3D network and form low dimensional structures where BX_6 octahedra only partially share their corners with neighbors. Low dimensional perovskites can be derived by slicing the parental 3D perovskite along different orientations (Fig. 1), which significantly affects both the structural and optoelectronic properties.[15–17] $\langle 100 \rangle$-oriented perovskites have the general formula $A'_2A_{n-1}M_nX_{3n+1}$, where A' indicates a bulky organic cation (*e.g.* an ammonium or sulfonium cation) and n is an integer (Fig. 1a). When $n = 1$, a two-dimensional 2D perovskite is formed where flat organic and inorganic sheets are stacked in alternation (Fig. 1a, left). Here, MX_6 octahedra share the 4 corners in an equatorial position, terminating the inorganic layers with the two under-coordinated halides in an apical position. For $n \geq 2$, the thickness of the inorganic perovskite layers is gradually increased by controlling the reaction stoichiometry, leading to the formation of "multidimensional" perovskites of the Ruddlesden–Popper series (Fig. 1a, right).[19,24] $\langle 110 \rangle$-oriented perovskites have the general formula $A'_2A_mM_mX_{3m+2}$ (Fig. 1b). When $m = 1$, one-dimensional (1D) perovskites are formed, characterized by chains of MX_6 units sharing two corners in an equatorial position (Fig. 1b, left). For $m = 2$, the resulting 2D perovskites are characterized by rippled inorganic layers terminated by two undercoordinated halides from each MX_6 octahedron, which therefore ends the layer exposing one edge (Fig. 1b, right). Lastly, $\langle 111 \rangle$-oriented perovskites with formula $A'_2A_{q-1}M_qX_{3q+3}$ form zero-dimensional (0D) structures (when $q = 1$) made of isolated MX_6 octahedra (Fig. 1c, left). The 2D perovskite ($q = 2$; Fig. 1c, right) is intrinsically different from the previous two classes, since B must be a trivalent cation to maintain electroneutrality. Here, the inorganic sheets are made of octahedra sharing three corners and terminating the inorganic slabs exposing one face, therefore contributing 3 undercoordinated halides to the terminating surface.[16] Thanks to the enormous synthetic versatility, a large number of alternative metal halide frameworks can be derived from the archetype structures shown in Fig. 1, for instance forming combinations of $\langle 100 \rangle$ and $\langle 110 \rangle$ perovskite frameworks or inducing different connectivity of corner-, edge- and face-sharing octahedra.[6]

1.2   Distortions of the perovskite lattice

The band structure, emissive properties and defect formation energy of perovskites are significantly affected by the connectivity of the inorganic motif.[25] The perovskite structural properties can be evaluated using some relevant parameters:

M–X–M angle and M–X bond length. While the M–X length has generally a secondary effect on the absorption properties of
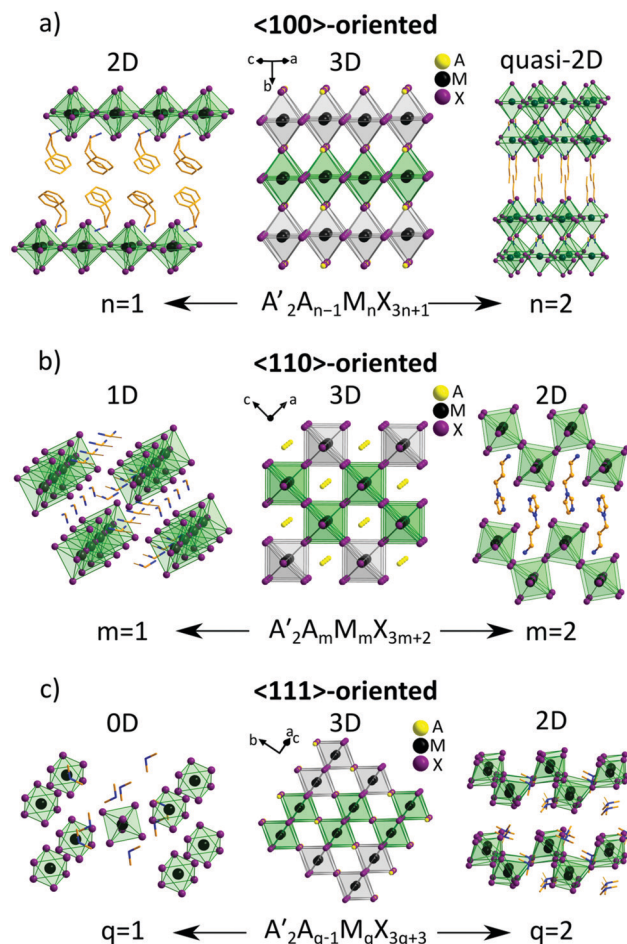

Fig. 1 Schematic representation of the derivation of low-dimensional perovskites from different cuts of the parental 3D perovskite. The archetype 3D lattice is shown in the centre viewed along different directions. (a) $\langle 100 \rangle$-oriented family $A'_2A_{n-1}M_nX_{3n+1}$: $n = 1$ (*e.g.* $(PEA)_2PbCl_4$, where PEA = phenethylammonium)[18] and $n = 2$ (*e.g.* $(NBT)_2(MA)Pb_2I_7$, where NBT = *n*-butylammonium and MA = methylammonium);[19] (b) $\langle 110 \rangle$-oriented family $A'_2A_mM_mX_{3m+2}$: $m = 1$ (*e.g.* $(IFA)_2(FA)SnI_5$, where IFA = iodoformamidinium and FA = formamidinium)[20] and $m = 2$ (*e.g.* $(API)PbBr_4$, where API = *N*-(3-aminopropyl)imidazole);[21] (c) $\langle 111 \rangle$-oriented family $A'_2A_{q-1}M_qX_{3q+3}$: $q = 1$ (*e.g.* $(DMA)_2SnCl_6$, where DMA = dimethylammonium)[22] and $q = 2$ (*e.g.* $(TMA)_3Sb_2Cl_9$, where TMA = trimethylammonium).[23]

the perovskite, the M–X–M angle has a major impact on the optical properties.[26] Considering the case of $\langle 100 \rangle$-oriented 2D perovskites, deviation of the M–X–M angle from the ideal geometry (180°) implicates distortions of the inorganic frameworks involving in-plane (θ_{in}) and out-of-plane (θ_{out}) tilt of the MX_6 octahedra.[27] The greater the tilt, the poorer the overlap between the metal and halide orbitals, widening the band-gap and causing the blue-shift of the absorption onset.[28,29]

Octahedral distortion. Distortions of the MX_6 octahedra combine deformations from the ideal O_h symmetry of M–X bond lengths (d_i), X–M–X angles (α_i), edges (X–X distances) and the volume (V),[29] which can also affect the luminescence properties of the material. For example, in the series $(C_4H_9NH_3)_2PbBr_4$, $(C_6H_5CH_2NH_3)_2PbBr_4$ and $(C_6H_5C_2H_4NH_3)_2PbBr_4$, the PL efficiency and lifetime decrease with the distortion of $PbBr_6$

octahedra as a consequence of the increase of the reduced mass of the excitons in relation to the structural distortion.[30] Octahedral distortion can be quantitatively evaluated by combining the octahedral angle variance σ_{oct}^2 and octahedral elongation λ_{oct},[31] which are defined as:

$$\sigma_{oct}^2 = \frac{1}{11} \sum_{i=1}^{12} (\alpha_i - 90)^2 \qquad (1)$$

$$\lambda_{oct} = \frac{1}{6} \sum_{i=1}^{6} (d_i/d_0)^2 \qquad (2)$$

where d_0 indicates the center-to-vertex distance of a regular polyhedron of the same volume. Alternatively, the octahedral distortion is also expressed by the distortion parameter Δ_d:[37]

$$\Delta_d = \frac{1}{6} \sum_{i=1}^{6} [(d_i - d_{av})/d_{av}]^2 \qquad (3)$$

where d_{av} is the average M–X bond length.

Octahedral connectivity. The connectivity of the MX_6 units is affected by the perovskite orientation, dimensionality and by the number of shared halide atoms between adjacent octahedra. The connectivity gradually increases from corner to edge and face-sharing octahedra, which results in band-gap widening and can modulate the confinement effects in low dimensional structures.[19,25,38]

2 Broadband emission in low dimensional perovskites

Low-dimensional perovskites behave like confined nanostructures,[6,15] where electronic and dielectric confinement arise from differences in the band-gap and polarizability of the organic and inorganic components. These conditions increase significantly the electron–hole Coulomb interaction (through the image charge effect) and the exciton binding energy (EBE) up to a few hundreds of meV,[39,40] so that the exciton population may become predominant compared to free-charges even at low excitation densities.[41] This is in net contrast to 3D perovskites, where a high dielectric constant and efficient Coulomb screening confer a remarkably low EBE (< 50 meV).[42,43] The resulting excitonic properties should then drive the characteristic photophysics, with the typical sharp excitonic absorption and extremely narrowband photoluminescence (full-width at half maximum FWHM $\sim$ 20 nm) characteristic of free-excitonic states.[40,44,45] However, many low dimensional perovskites show the opposite behavior,[46,47] with ultra-broadband (FWHM beyond 100 nm) and highly Stokes shifted photoluminescence (>1 eV) arising from intra-gap states with a wide energy distribution.[7,48] The perovskite dimensionality, connectivity and structural distortions contribute to shape the energetic landscape in these materials, ultimately determining their emissive properties; the following paragraphs summarize a wide range of experimental evidence to rationalize such a structure/photophysics relationship.

2.1 2D perovskites

$\langle 100 \rangle$-oriented 2D perovskites display a complex trend in their photoluminescence since the balance between narrowband and broadband room-temperature emission appears to be strongly related to their structural properties. While structures with close-to-ideal geometries show exclusively free-excitonic emission (*e.g.*, BA_2PbBr_4, where BA = *n*-butylammonium), more distorted structures have a prominent contribution from broadband PL (*e.g.* $(EDBE)PbCl_4$ (Fig. 2a), where EDBE = 2,2-(ethylenedioxy)bis(ethylammonium)).[7,8] While this has been mainly studied in lead-based perovskites, similar behaviour has also been observed in cadmium-based ones $(C_6H_{11}NH_3)_2[CdBr_4]$.[49] In intermediate cases, the combination of narrow/broadband PL with comparable intensity can be observed. This is the case of (*cis*-CyBMA)$PbBr_4$ (*cis*-CyBMA = 1,3-bis(methylamino)cyclohexane) (Fig. 2b and c) and $(2meptH_2)PbBr_4$ (2mept = 2-methyl-1,5-diaminopentane), which have $PbBr_6$ octahedra with close-to-ideal geometry but feature a relevant octahedral tilt with a Pb–Br–Pb average bond angle $<150°$ (Fig. 2b).[32,50–52] Recently, M. D. Smith *et al.* rationalized the structure/optical property relationship by examining the ratio between the intensities of the broad emission (I_{BE}) and the narrow emission (I_{NE}) in a set of eight $\langle 100 \rangle$-oriented bromide perovskites.[47,53] Within this dataset, it was found that the relative intensity of the broad emission (given by the ratio I_{BE}/I_{NE}) increases with the increase of out-of-plane distortion of the Pb–(μ-Br)–Pb angle, with the exception of $(CEA)_2PbBr_4$ (CEA = cyclohexylammonium), which shows room temperature broadband emission despite the absence of an out-of-plane tilt. On the other hand, an unequivocal correlation of the I_{BE}/I_{NE} ratio with the octahedral distortion was not clearly identified.[27,53] The structural properties play a similar role also in the multidimensional series $EA_4Pb_3Br_{10-x}Cl_x$ (Fig. 2d); here distortions of the octahedral coordination as well as the octahedral tilt increase from $x = 0$ to $x = 10$, allowing one to reach white PL in $EA_4Pb_3Cl_{10}$ (Fig. 2d) compared to the blue emission of $EA_4Pb_3Br_{10}$.[33]

The corrugated $\langle 110 \rangle$-oriented perovskites usually endure important steric hindrance effects from the templating cations, which result in highly distorted geometries. Moreover, the presence of two undercoordinated halides at the organic/inorganic interface allows large lattice rearrangements, easing the formation of photoinduced defects or structural rearrangements. As a consequence, all the reported bromide-based $\langle 110 \rangle$ perovskites show a prominent contribution of broadband emission at room temperature. These include $(API)PbBr_4$ and $(AETU)PbBr_4$ [API = *N*-(3-aminopropyl)imidazole and AETU = *S*-(aminoethyl)isothiourea],[21,54] (*N*-MEDA)$PbBr_4$ [*N*-MEDA = *N*1-methylethane-1,2-diammonium][55] and $(EDBE)PbBr_4$.[8] The latter shows a photoluminescence quantum yield of 9%, which is the highest reported among bulk 2D perovskites. Similar broadband emission was reported by L. Mao *et al.* in α-$(DMEN)PbBr_4$ [DMEN = 2-(dimethylamino)-ethylamine], featuring a 3×3 corrugated structure of the $\langle 110 \rangle$-type (Fig. 2e). In comparison with other 2D bromide perovskites based on DMAPA = 3-(dimethylamino)-1-propylamine and DMABA = 4-dimethylaminobutylamine, the authors identified a correlation between increased octahedral distortion and PL
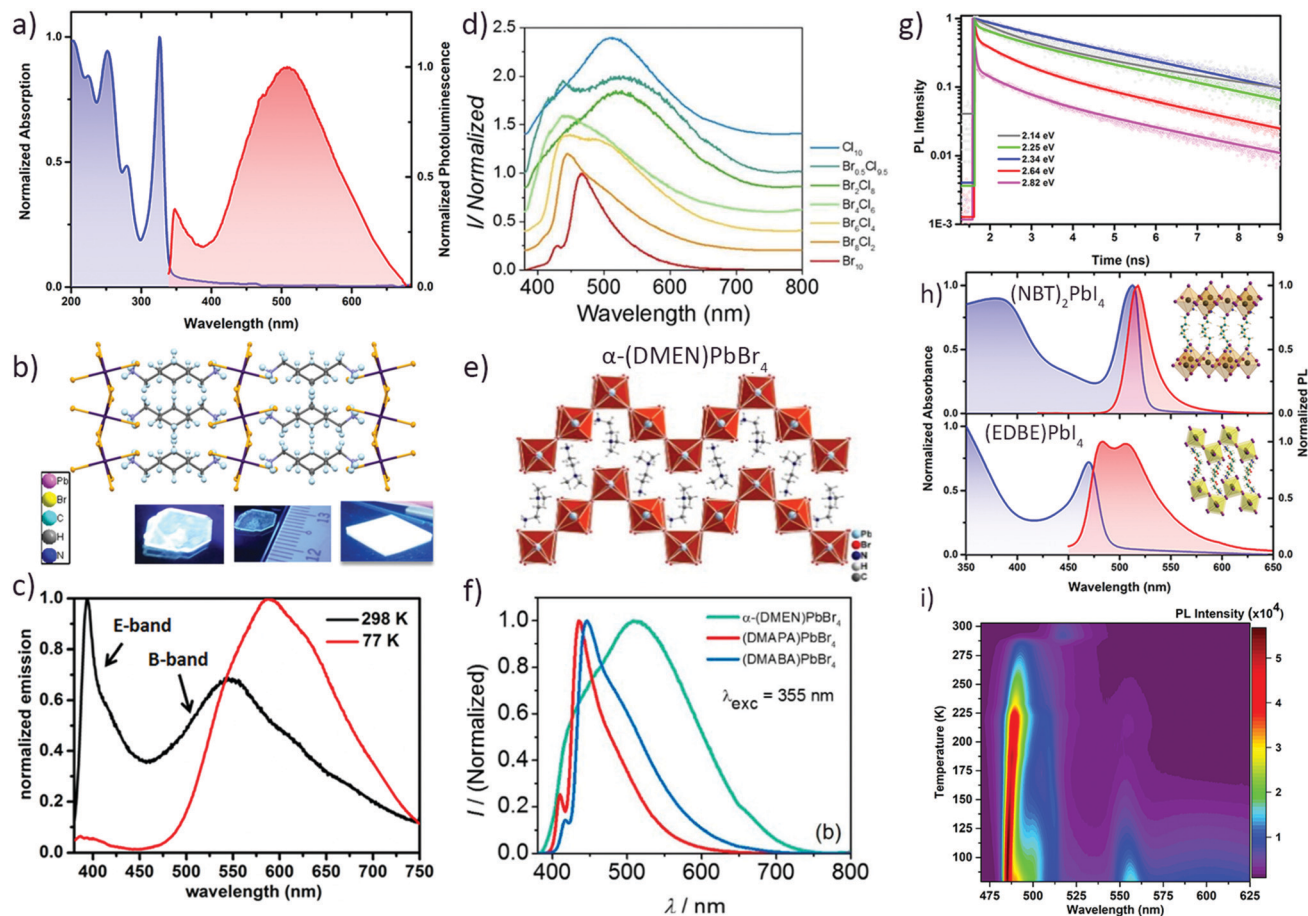
Fig. 2 (a) Steady state absorption and PL of (EDBE)PbCl$_4$; adapted from ref. 7 with permission from The Royal Society of Chemistry. (b and c) Crystal structure and characteristic white light emission of (cis-CyBMA)PbBr$_4$ and the corresponding temperature dependent steady state photoluminescence; reproduced with permission from ref. 32 Copyright 2017, Wiley-VCH Verlag GmbH & Co. KGaA, Weinheim. (d) PL trend of the multidimensional series EA$_4$Pb$_3$Br$_{10-x}$Cl$_x$; reprinted with permission from ref. 33 Copyright 2017 American Chemical Society. (e and f) Crystal structure of α-(DMEN)PbBr$_4$ and photoluminescence spectra of α-(DMEN)PbBr$_4$, (DMAPA)PbBr$_4$, and (DMABA)PbBr$_4$ (λ_{exc} = 355 nm); reprinted with permission from ref. 34 Copyright 2017 American Chemical Society. (g) Time-resolved photoluminescence of (EDBE)PbCl$_4$; reproduced from ref. 7 with permission from The Royal Society of Chemistry. (h) Optical properties of (NBT)$_2$PbI$_4$ and (EDBE)PbI$_4$ – the insets show their corresponding crystal structures; adapted with permission from ref. 35 Copyright 2016 American Chemical Society. (i) Temperature dependent PL of (NBT)$_2$PbI$_4$; reproduced from ref. 36 with the permission of AIP Publishing.

broadening (Fig. 2f).[34] Despite some variability between different compounds, the broadband emission in ⟨100⟩ and ⟨110⟩-oriented bromide-based 2D perovskites shares some common characteristics: it is typically centered in the range 500–560 nm, is highly Stokes shifted (>1 eV), and has a FWHM up to 160 nm and photoluminescence decay varying across the emission spectrum (Fig. 2g) reported in the range 0.4–15 ns, pointing to the presence of multiple emissive color centers.[7] On the other hand, iodide-based perovskites show a slightly different scenario. For example, the ⟨110⟩-oriented iodide perovskite (EDBE)PbI$_4$ does not show white light emission at room temperature, however it is also characterized by a considerable broadening of the excitonic emission (FWHM = 70 nm), which correlates with the increased structural distortion compared to purely free-excitonic emitting iodide-based 2D perovskites (Fig. 2h).[35] At low temperature, highly Stokes shifted broadband luminescence centered around 600–625 nm was also observed in

alkylammonium-based iodide perovskites such as (NBT)$_2$PbI$_4$ (NBT = n-butylammonium; Fig. 2i), DA$_2$PbI$_4$ (DA = dodecyl-ammonium) and HA$_2$PbI$_4$ (HA = hexylammonium). Here, the broadband emission was measured only below 200 K and no evident correlation between the octahedral tilt and the appearance of broadband emission was observed.[36,56]

In ⟨111⟩-oriented perovskites, the presence of three under-coordinated halides at the organic/inorganic interface further eases structural distortions and coordination rearrangements, suggesting that they should also be prone to broadband emission. Being based on trivalent cations Sb^{3+} and Bi^{3+},[57,58] they also present some differences compared to the previous two perovskite types (e.g. the PL is usually more red-shifted), although only a few examples are available. While Rb$_3$Bi$_2$I$_9$ shows no PL response (probably due to the predominance of non-radiative recombination pathways), Cs$_3$Sb$_2$I$_9$ films display highly Stokes shifted PL peaked at

This journal is © The Royal Society of Chemistry 2019

J. Mater. Chem. C, 2019, 7, 4956–4969 | 4959

646 nm, with a FWHM of ~60 nm and a complete lack of free-exciton emission.[59]

Even though structural deformations appear to strongly impact the luminescence characteristics of this class of perovskites, a unified model describing how the structural properties shape the energetic landscape of 2D perovskites with different orientation and composition is still missing. Similarly, the reports supporting the relative contributions of octahedral distortion or tilt to the broadening process are sometimes conflicting, leaving space for further investigations. Synthesis of new materials and photophysical characterization should provide new insights to guide the crystal engineering of layered perovskites with controlled optical properties.
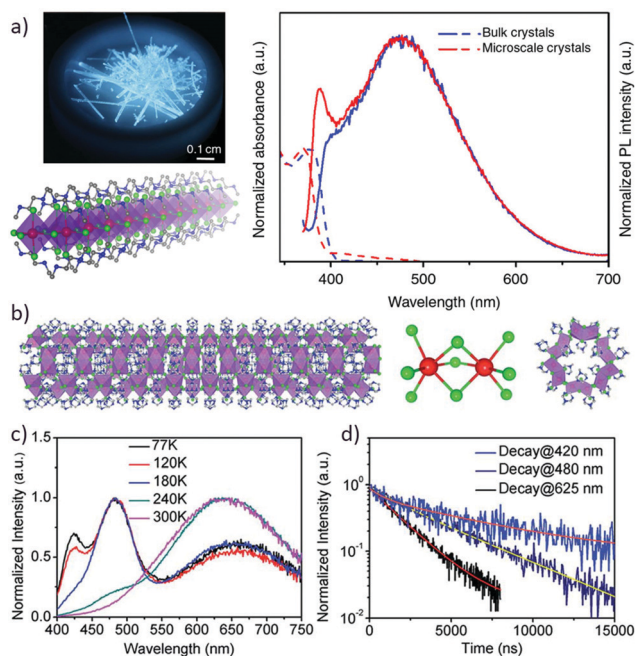
2.2 1D and 0D perovskites

Z. Yuan *et al.* discovered that the cation *N,N′*-dimethyl-ethylenediammonium (DMEDA) templates the growth of the pseudo-1D perovskite (DMEDA)PbBr$_4$, in which lead bromide wires are composed of double edge-sharing PbBr$_6$ octahedra, surrounded by a shell of DMEDA^{2+} cations (Fig. 3a).[60] The material could be synthesized in the form of bulk crystalline needles having similar emission to that characteristic of layered perovskites: highly Stokes shifted (1 eV), cold bluish white light centered at 475 nm with a PLQY up to 18–20% and a lifetime of 37.3 ns at room temperature (Fig. 3a). The corresponding chloride perovskite (DMEDA)PbCl$_4$ displayed excitation-dependent broad photoluminescence, attributed to the competition between different emission centres.[62] The use of DMEDA

Fig. 3 (a) White light emission, crystal structure and optical properties of (DMEDA)PbBr$_4$; reproduced with permission from ref. 60 Copyright 2017 Springer Nature. (b) Structure of (HMTA)$_3$Pb$_2$Br$_7$ nanotubes and the corresponding (c) steady state and (d) time-resolved photoluminescence (77 K); reproduced with permission from ref. 61 published by The Royal Society of Chemistry.

with Sn^{2+} was also reported to form the 0D perovskites (DMEDA)$_4$SnBr$_6$ and (DMEDA)$_4$SnI$_6$ with orange and red emission, FWHM > 100 nm and Stokes shift ~200 nm.[63] In particular, the iodide-based perovskite showed an exceptionally long PL lifetime of 1.1 μs and an extremely high PLQY up to 95% at room temperature, which was ascribed to the increased quantum confinement in the 0D structure.[46] PL enhancement by means of decreased dimensionality has also been exploited to obtain warm white-light with a remarkably high PLQY (up to 86%) in lead-free double perovskites such as Cs$_2$AgInCl$_6$.[64] Despite being formed by a continuous metal halide network, the presence of alternating AgCl$_6$ and InCl$_6$ octahedra breaks the continuity of orbital overlap resulting in a reduced 0D-like electronic dimensionality.[65] Charge confinement within single octahedral units was further enhanced by means of Na$^+$ and Bi^{3+} doping.[64] Hexamethylenetetrammonium (HMTA) was used for the synthesis of (HMTA)$_3$Pb$_2$Br$_7$, which forms a bulk assembly of 1D lead bromide nanotubes: six dimers of face sharing lead bromide octahedra (Pb$_2$Br$_9^{5-}$) connect at the corners forming a ring with an inner radius of 4 Å which extends in one dimension to form the nanotube (Fig. 3b).[61] Here, lead bromide octahedra are highly distorted, with Pb–Br bonds in the range 2.873–3.163 Å and a Br–Pb–Br angle between 77.25° and 113.15°. Photoexcitation between 250 and 400 nm resulted in broadband emission (FWHM = 158 nm) peaked at 580 nm with PLQY = 7% and a long lifetime of 106 ns. Cooling at 77 K allowed three distinct emission peaks centered at 420, 480 and 625 nm to be resolved with a lifetime of 7, 4.0 and 1.8 μs, respectively, suggesting that multiple species are involved in the emission process (Fig. 3c and d). Ethylene-diamine and piperazine were also shown to template pseudo 1D and 0D structures with broadband emission.[66]

2.3 Exotic metal halide frameworks

Photoluminescence broadening was also shown in various examples of more complex lead halide frameworks, suggesting a relation with the nature of the metal halide bonds rather than to the intrinsic properties of the perovskite structure. For example, trimethylphenylammonium (TMPA) and a series of sulfonium cations including trimethylsulfonium (TMS) and butane-1,4-bis(dimethylsulfonium) (1,4-BBDMS) were shown to template structures in which isolated trimers or pentamers of face-sharing lead bromide octahedra are surrounded by the organic cations.[67] These materials have similar optical properties, exemplified by the case of (1,4-bbdms)$_3$Pb$_3$Br$_{12}$ in Fig. 4a and b: excitonic properties comparable to those of standard 2D perovskites, highly Stokes shifted (>1.7 eV) red photoluminescence centered at 690 nm and FWHM ~ 0.7 eV. Such broadband red luminescence appears to be characteristic of this type of connectivity of the inorganic framework, where octahedra are connected through one of their faces. Interestingly, white light luminescence was also achieved in the 3D haloplumbate frameworks (H$_2$DABCO)(Pb$_2$Cl$_6$) and (H$_3$O)(Et$_2$-DABCO)$_8$ (Pb$_{21}$Cl$_{59}$), where DABCO = 1,4-diazabicyclo[2.2.2]-octane and Et = ethyl (Fig. 4c and d).[68] In this case, white light emission was obtained by combining blue photoluminescence of the organic cation

4960 | *J. Mater. Chem. C,* 2019, **7**, 4956–4969
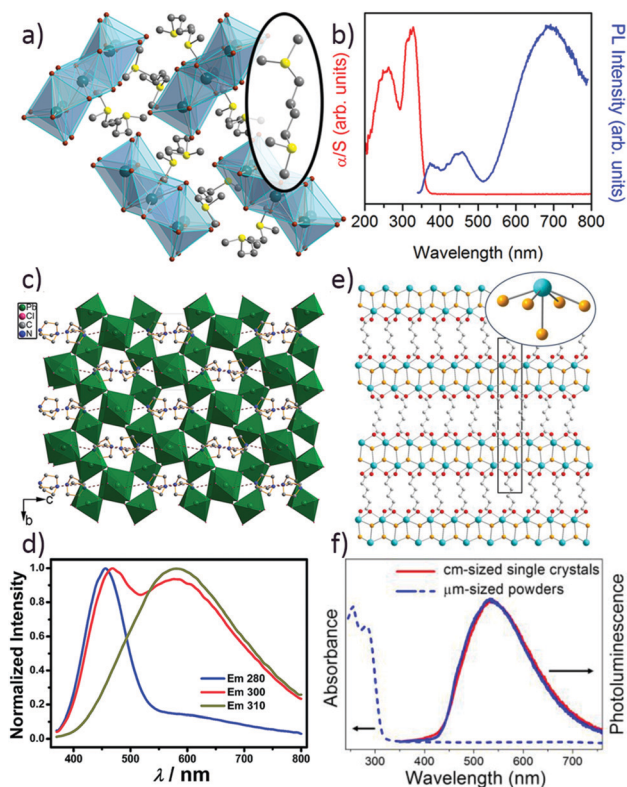
This journal is © The Royal Society of Chemistry 2019

Fig. 4 (a) Crystal structure and (b) transformed diffuse reflectance and photoluminescence (λ_{exc} = 350 nm) of (1,4-bbdms)$_3$Pb$_3$Br$_{12}$; reprinted with permission from ref. 67 Copyright 2017 American Chemical Society. (c) Crystal structure and (d) normalized photoluminescence at different excitation wavelengths of (H$_2$DABCO)(Pb$_2$Cl$_6$); reproduced from ref. 68 with permission from The Royal Society of Chemistry. (e) Crystal structure and (f) absorption and emission spectra of [Pb$_2$Cl$_2$]$^{2+}$[$^-$O$_2$C(CH)$_2$CO$_2$$^-$]; reproduced with permission from ref. 69 Copyright 2017, Wiley-VCH Verlag GmbH & Co. KGaA, Weinheim.

with broad yellow emission originating from the lead chloride network, respectively centered at 455 and 585 nm in (H$_2$DAB-CO)(Pb$_2$Cl$_6$). Despite the modest PLQY (1–2.5%), a very high color rendering index (CRI) value was achieved (96) together with an electric conductivity up to 2.83 × 10^{-7} S cm^{-1}.

S. Z. Zhuang *et al.* recently synthesized a series of rare cationic layered lead halides with formula [Pb$_2$X$_2$]$^{2+}$[$^-$O$_2$C-(CH)$_2$CO$_2$$^-$] (X = F, Cl, and Br) by a hydrothermal reaction, where corrugated cationic lead halide sheets are held in place by elongated adipate anions (Fig. 4e and f).[69] These materials differ from standard 2D perovskites since the carboxylate is directly coordinated to the Pb^{2+} centres through covalent bonds. In the fluoride compound the Pb^{2+} is further coordinated with four fluorine atoms forming a distorted square-planar geometry, while the chloride and bromide compounds form PbX$_5$ units which are analogous to half of the PbX$_6$ octahedra of typical 2D layered perovskites. Setting aside the contribution of the uncoordinated axial ligands, the PbX$_5$ units of the Cl and Br-substituted materials showed remarkable octahedral distortion, with λ_{oct} = 87.9 and λ_{oct} = 25.2, respectively. In agreement with the extremely distorted geometry, all the

compounds of the series display broadband PL centered between 536 and 565 nm, a FWHM up to 0.70 eV (167 nm) and an average PL lifetime in the range 2.24–2.64 ns (Fig. 4f). [Pb$_2$Br$_2$][O$_2$C(CH)$_2$CO$_2$] reached the highest PLQY of 11.8% and CRI of 68. In a similar way, adipate and succinate were used for the synthesis of unusual 3D cationic metal halide frameworks with formula [Pb$_2$Br$_2$][O$_2$C(CH$_2$)$_4$CO$_2$] and [Pb$_3$Br$_4$][O$_2$C(CH$_2$)$_2$CO$_2$], where the different electronegativity of oxygen and bromine, as well as the shorter bond length of Pb–O compared to Pb–Br, leads to extremely distorted Pb^{II} centers.[70] Consistently with the previous cases, such distorted 3D cationic frameworks showed white light emission with a FWHM up to 0.88 eV (166 nm), a lifetime of about 1.7 ns and a PLQY up to 5.6%.[70]

3 Origin of broadband emission

The observation of such a dominant contribution of broadband, highly Stokes shifted emission in low-dimensional perovskites has stimulated the scientific community to identify the physical processes underlying this phenomenon. Mechanistic studies performed on several metal halides reveal common characteristics which point to the formation of self-trapped excitons, which define the emissive intra gap states (see Section 3.1 for a detailed description).[71] In this regard, the main observations include: (i) the emission bandwidth and PLQY are unrelated to the perovskite crystal size, remaining substantially unchanged in films, powders and nanocrystals, excluding the involvement of surface/edge states in the emission process.[8,70,72] (ii) The integrated PL intensity of broadband emission linearly increases with the excitation intensity over several orders of magnitude without showing saturation, ruling out the contribution of permanent defects (particularly in Cl and Br perovskites).[8,62,63,67] (iii) The PL temperature dependence is consistent with the presence of an energy barrier for the self-trapping process, which is expected given the structural rearrangement necessary to induce charge localization.[73] The contribution of broadband PL increases at lower temperature with respect to free-excitonic emission, accompanied by an increase of the overall luminescence efficiency.[32,50] This result from the lower probability of exciton de-trapping jointly with the reduction of the impact of non-radiative recombination.[7,47,51] When the temperature is further reduced (usually below ∼80 K), the free excitons become progressively unable to overcome the energy barrier to undergo self-trapping, and the relative contribution of free-excitonic emission starts to increase again.[47,52,53,73] (iv) Transient absorption measurements revealed the formation of an unstructured photoinduced absorption band covering the entire visible spectral region, pointing to the formation of multiple emissive color centers distributed throughout the perovskite band-gap. On the contrary, narrowband emitters show bleaching features below the excitonic absorption corresponding to the filling of trap states.[7,51] (v) Transient absorption and ultrafast terahertz (THz) pump–probe reveal the ultrafast formation of the emissive species in the timeframe <100 fs.[7,51] This is comparable to the vibration of the Pb–X framework,

suggesting its involvement in the trapping process. This is further supported by the PL narrowing at low temperature, consistent with the coupling to vibrational modes of the inorganic lattice.[8,49,60,69,70]

3.1 Intrinsic self-trapping and polaron formation in metal halide semiconductors

Similar to crystalline inorganic materials, when an electron is added to an ionic and highly polar crystal,[74] the strong Coulomb interactions between the excess charge and the lattice ions enhance the electron–phonon couplings. In this case, electrons are delocalized over several lattice sites, forming so-called large polarons (also known as Fröhlich polarons).[75,76] In the case of 3D perovskites, the view is rapidly emerging (currently under vibrant debate) that reorientation of the organic cations[77] and deformation of the $PbBr_3^-$ inorganic frameworks[78] can stabilize and localize charge carriers with the polarization cloud spanning many unit cells, thus forming large polarons.[79] These large polarons have optical signatures in the THz frequency range,[78,80,81] which can screen the Coulombic potential and reduce trapping and carrier scattering in 3D hybrid perovskites.[82] In $MAPbX_3$, lattice displacement after photoinduced carrier generation was probed through impulsive vibrational spectroscopy, providing further experimental evidence of the polaronic nature of the photoexcitation.[83,84]

In low-dimensional systems, the coulombic and dielectric confinement sustain tightly bound excitons which interact with the highly polar lead halide framework. Recently, strong photo-induced lattice deformations have been identified in several 2D perovskites, where excitonic polarons must be considered to account for their characteristic luminescence and absorption line-shapes.[87,88] The strong exciton–phonon coupling can ease exciton self-trapping, leading to the photoinduced generation of small polarons in which the excess charges are spatially confined to one crystal unit cell or less.[89] In this case, the short-range deformation potential due to the changes in local bonding related to the excess charge plays the dominant role. Due to their strongly confined nature, the formation of such polaronic species is highly dependent on the local structural properties of the crystal lattice,[35] similar to the case of halide-bridged mixed-valence transition metal linear chain complexes.[90] These small polarons can be viewed as self-trapped holes or electrons,[71] as often observed in alkali, alkaline-earth, and perovskite-structure halides, and demonstrated in early work on lead halides ($PbBr_2$ and $PbCl_2$) using electron paramagnetic resonance (EPR).[91–95] Because of the strong lattice deformation associated with the trapping process, the excited state is shifted compared to the ground state, and radiative decay results in broad and highly Stokes shifted luminescence.[52,71,73] In a similar way, in 2D hybrid perovskites the broadband emission can be interpreted as the superimposed, homogeneously broadened luminescence from a series of multiple polaron-exciton states.[7,48] As shown in Fig. 5a, we have simulated the photo-generation of small polarons and charge self-trapping effects in 2D hybrid perovskites by exerting local perturbations onto the 2D perovskite periodic models.[7] By shortening selected bond
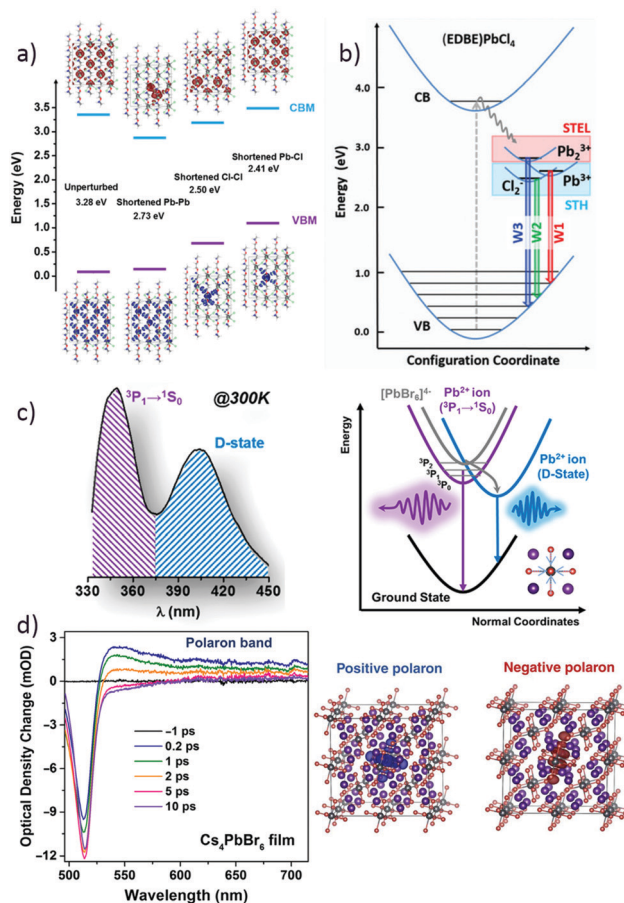

Fig. 5 (a) Energy levels marking the valence band maximum (VBM) and conduction band minimum (CBM), and corresponding charge density distributions for the (EDBE)$PbCl_4$ supercell without and with lattice perturbations; reprinted with permission from ref. 48 Copyright 2017 American Chemical Society. (b) Schematic representation of the emissive process *via* polaron formation in white-light generation for (EDBE)$PbCl_4$; reproduced from ref. 7 with permission from The Royal Society of Chemistry. (c) Steady-state photoluminescence spectra of Cs_4PbBr_6 nanocrystals and the diagram of $^3P_1$ to $^1S_0$ and D-state emission from Pb^{2+} ions; reprinted with permission from ref. 85 Copyright 2017 American Chemical Society. (d) Transient absorption spectra of Cs_4PbBr_6 thin film with different delay times using 310 nm excitation and charge density distributions within the central [$PbBr_6$]$^{4-}$ octahedron for positive and negative polarons in the Cs_4PbBr_6 supercell; reprinted with permission from ref. 86 Copyright 2017 American Association for the Advancement of Science.

lengths (*i.e.* Pb–Pb, Pb–X and X–X) to create the local structural deformations, we found that (i) the Pb–Pb dimerization leads to the formation of a self-trapped electron at Pb_2^{3+} sites; (ii) the hole density is highly localized at the Cl–Cl or Br–Br pairs, showing the formation of V_k centers (Cl_2^- and Br_2^-); and (iii) holes localize at a single Pb atom, leading to the formation of Pb^{3+} centers coupled with the lattice deformation. Therefore, the strong interaction between charge carriers and phonons can yield the formation of self-trapped electron (STEL, Pb_2^{3+}) and self-trapped hole (STH, Pb^{3+} and X_2^-) states. These STEL and STH, consisting of charges trapped at specific sites of the inorganic lattice by their own distortion field, define a series of intra-band polaronic emissive states which decay radiatively

4962 | *J. Mater. Chem. C,* 2019, **7**, 4956–4969

This journal is © The Royal Society of Chemistry 2019

with broadband emission (see Fig. 5b).[7] We have also considered a molecular-cluster model to characterize the actual small polaron distributions in 2D hybrid perovskites.[48] The resulting charge density distribution confirms that the local structural change induces the formation of a localized, positive small polaron (Pb^{3+} self-trapped hole). The strongly localized additional electron density surrounding Pb^{2+} induced large repulsive interactions between adjacent Pb and Cl atoms, thus markedly deforming the local geometry of the 2D perovskite clusters.[48] Similarly, the formation of V_k centers and electron polarons was proposed to explain the scintillation properties of Cs_2HfCl_6.[96] Recently, X. Wang et al. showed by means of density functional theory calculations that reduced electronic dimensionality plays a crucial role in the formation of self-trapped excitons.[65] Although several species can form, it was proposed that self-trapped excitons connected to Jahn–Teller-like octahedral distortion give the main contribution to the broadband luminescence,[65] while all other types of self-trapped excitons act as non-radiative recombination channels. The existence of two such competing mechanisms suggests that Jahn–Teller-like self-trapped excitons must be promoted while suppressing non-Jahn–Teller-like states in order to obtain high photoluminescence quantum yields.[65] This represents a step forward in the establishment of a general structure–property relationship in systems with different structural dimensionality and accounts for the experimental observation of broadband emission primarily in the most distorted structures.

Broadband emission can also be achieved in the high-energy spectral region in 0D Cs_4PbBr_6 nanocrystals (see Fig. 5c).[85] However, the origin of such emission is different from 2D hybrid perovskites: the UV emission around 350 nm can be assigned to the allowed optical transition of $^3P_1$ to $^1S_0$ in Pb^{2+} ions and the low-energy UV emission at approximately 400 nm to the charge transfer state involved in the 0D host lattice (i.e. the D-state). In this case, we can effectively tune the Pb^{2+} ion emission in the visible spectral region by adopting different 0D perovskite host lattices. 0D perovskites are also ideal platforms for studying photogenerated small polarons since the complete isolation of the octahedra is expected to strengthen electron–phonon interactions.[86] As shown in Fig. 5d, the femtosecond transient absorption of Cs_4PbBr_6 thin film shows a new positive broad band appearing above 530 nm, due to polaron absorption. The hole charge density is highly localized at the central site once the Pb–Br bonds of the central $[PbBr_6]^{4-}$ unit are shortened, leading to the formation of Pb^{3+} centers coupled with the lattice deformation. The individual $[PbBr_6]^{4-}$ octahedra in the 0D crystal can be easily perturbed by photoexcitation processes, generating polaronic states through structural deformation potentials. These results suggest that the increased electron–phonon coupling in low-dimensional perovskites can facilitate small polaron generation providing important optical fingerprints, like broadband emission and polaron band absorption.

3.2 The role of extrinsic defects

The previous paragraph discussed cases of intrinsic self-trapping, purely polaronic effects in a perfect crystal where a carrier is bound within a potential well arising from the displacement of the surrounding atoms to new equilibrium positions. However, the presence of permanent defects (e.g. vacancies, interstitial atoms or impurities) can aid the trapping process, and a charge might localize on one of several symmetry equivalent ions neighboring a defect.[89] In some cases, this trapping might retain a polaronic character leading to a phenomenon identified as extrinsic self-trapping.[97] This is the case, for example, of electron trapping at oxygen vacancies in HfO_2,[98,99] charge trapping in amorphous SiO_2,[100] hole trapping at Mg^{2+} vacancies in MgO_2 or small polarons in doped $LaMnO_3$.[89,101] Given the relevance of defects in determining the photophysical behavior of 3D perovskites,[102–104] it is likely that extrinsic trapping might play a role also in low-dimensional perovskites.

While Cl and Br based low-dimensional perovskites have been mainly discussed in terms of intrinsic self-trapping,[47,105] iodide-based 2D perovskites have offered hints for discussion of the role of permanent defects. For example, in $(EDBE)PbI_4$ the PL power dependence shows a monotonic reduction, indicating its relation with permanent defects which are saturated at higher excitation densities.[35] Here, ab initio calculations showed that the partial oxidation of two iodine atoms in proximity to a Pb vacancy can form stable V_F centers, consisting of I_3^- trimers stabilized by a vicinal lead vacancy (Fig. 6); overall, the process involves the trapping of two holes in proximity to the point defect, further inducing a local structural rearrangement coupled to the charge localization.[35] On the other hand, iodide interstitials have been proposed to play a role in the radiative recombination process leading to the broadband emission in HA_2PbI_4 and DA_2PbI_4.[56] We note that in ⟨111⟩ 2D and 0D perovskites such as $Cs_3Sb_2I_9$ and $Cs_3Bi_2I_9$, PL power dependence with both linear and sublinear behavior has been reported.[59,106] This leaves open questions on the possibility of intrinsic self-trapping,[59] while inviting the reconsideration of the role of extrinsic defects and trap assisted emission in these systems.[106]

3.3 Future perspectives

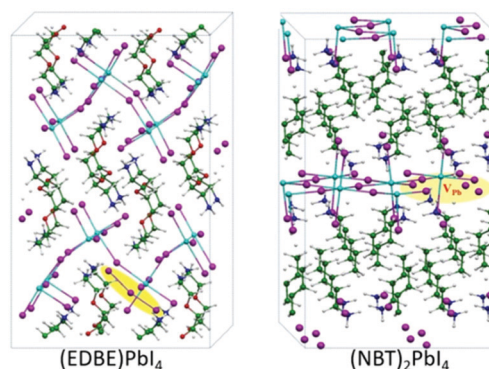From a fundamental standpoint, several questions remain open. While simulations and preliminary experimental results

Fig. 6 Geometry of a neutral Pb vacancy in different perovskite structures. While $(EDBE)PbI_4$ favors the formation of I_3^- close to a Pb vacancy (left), such structural rearrangement is energetically unfavorable in $(NBT)_2PbI_4$ (right); reproduced with permission from ref. 35 Copyright 2016 American Chemical Society.

point towards the relevance of charge localization effects, the interplay between intrinsic self-trapping and defect-related trapping, as well as the contribution of optical and acoustic phonons to the trapping process, needs to be elucidated, and additional experimental techniques will be necessary to further validate the formation of small polarons. For example, direct evidence for the formation of self-trapped excitons and their induced local lattice distortion might come from electron paramagnetic resonance (EPR), neutron diffraction measurements and scanning tunneling microscopy.[107,108] Infrared photoinduced absorption is also expected to reveal typical infrared active vibrational (IRAV) modes in low-energy spectral regions, characteristic of charged polaronic species.[79,109] Formation of small polarons is also expected to lead to thermally activated transport, with a mobility increase at higher temperature,[110] while time resolved photocurrent will be necessary to probe the polaron formation, relaxation and dynamics on different time scales. At this stage, the transport properties of these low-dimensional materials remain largely unexplored, despite their strong relevance for future application in optoelectronic devices.

4 Applications of broadband polaronic emitters

The structural properties of low-dimensional metal halide perovskites can be synthetically engineered to modulate the PL energy and bandwidth, making them highly attractive for solid-state lighting (SSL) and integration in light emitting diodes and transistors. Table 1 and Fig. 7 summarize the luminescence properties for different types of broadband emitting

perovskites in terms of the color rendering index (CRI), correlated colour temperature (CCT), Commission Internationale de l'Eclairage (CIE) chromaticity coordinates and PLQY.[68,111] In particular, the achievement of high CRI values (>80) is required for human eye-friendly and color-critical high-level applications and is crucial to make SSL competitive against conventional lighting and display systems. Nowadays, white-light emission in solid state devices is typically achieved by mixing different phosphors, leading to issues regarding poor color rendition, self-absorption and different degradation rates.[112,113] Broadband emitting perovskites are ideal candidates for application in single emitter white-light LEDs, helping to avoid the aforementioned issues. Although excellent CRI values were achieved with 3D haloplumbate frameworks and 2D perovskites, their PLQY is still low ($<9\%$) for practical applications. Among layered perovskites, the $\langle 100 \rangle$ type with strong octahedral distortion provides the highest CRI values, although the PLQY is generally low. This suggests that the strong structural distortion necessary to favor exciton self-trapping in 2D perovskites also opens additional non-radiative relaxation pathways, partially quenching the luminescence. Increased quantum confinement effects in lower dimensional structures ease the formation of self-trapping phenomena and substantially increase the emission efficiency and PL lifetime, but tend to red-shift the luminescence (Table 1 and Fig. 7), worsening the quality of the white-light emission. To date, (EDBE)PbBr$_4$ microcrystals, (DMEDA)SnBr$_6$, (PEA)$_2$PbBr$_x$Cl$_{4-x}$ and Cs$_2$Ag$_{0.60}$Na$_{0.40}$InCl$_6$ have been employed for fabrication of white-light emitting LEDs using a down-conversion approach, where a UV commercial LED was used to excite the perovskite.[63,64,114] As an alternative approach for the emission

Table 1 Reported room temperature luminescence properties of broadband emitting metal halide frameworks

Templating cation	Perovskite	CIE (x, y)	CRI	CCT	Broadband PL lifetime (ns)	PLQY (%)	Ref.
3D haloplumbate framework	(H$_2$DABCO)(Pb$_2$Cl$_6$)	(0.33, 0.34)	96	5393	18 (λ_{em} = 585 nm)	2.5	68
	(H$_3$O)(Et$_2$-DABCO)$_8$(Pb$_{21}$Cl$_{59}$)	(0.38, 0.31)	88	3496	54 (λ_{em} = 690 nm)	1.0	68
Cationic 3D lead halide	[Pb$_2$Br$_2$][O$_2$C(CH$_2$)$_4$CO$_2$]	(0.33, 0.48)	56^a	5727	1.7 (λ_{em} = 530 nm; av)	5.6	70
	[Pb$_3$Br$_4$][O$_2$C(CH$_2$)$_2$CO$_2$]	(0.25, 0.32)	72^a	11 967	1.6 (λ_{em} = 480 nm; av)	1.8	70
Multidimensional perovskite	(EA)$_4$Pb$_3$Br$_{0.5}$Cl$_{9.5}$	(0.30, 0.35)	83	7132	1.21 (av)	—	33
$\langle 100 \rangle$ 2D perovskite	(EDBE)PbCl$_4$	(0.33, 0.39)	81	3990	0.04–3.8	2.0	7 and 8
	(AEA)PbBr$_4$	(0.29, 0.34)	87	—	—	—	53
	(CEA)$_2$PbBr$_4$	(0.48, 0.45)	82	2695	—	—	52
	(cis-CYBMA)PbBr$_4$	(0.31, 0.34)	94	6785	1.2–2.2	1.6	32
	(PEA)$_2$PbCl$_4$	(0.37, 0.42)	84	4426	3 (λ_{em} = 545 nm; av)	<1	72
	(2meptH$_2$)PbBr$_4$	(0.24, 0.23)	91	—	2.23 (av)	3.37	50
$\langle 110 \rangle$ 2D perovskite	(EDBE)PbBr$_4$	(0.39, 0.42)	84	5509	14 (λ_{em} = 570 nm) 0.04–3.24	9.0	8 7
	(N-MEDA)[PbBr$_4$]	(0.36, 0.41)	82	4669	1.2	1.5	55
	(API)PbBr$_4$	(0.24, 0.32)^a	65^a	11 702^a	—	—	21
	(AETU)PbBr$_4$	(0.16, 0.18)^a	—	>100 000^a	—	—	54
3×3 $\langle 110 \rangle$ 2D perovskite	α-(DMEN)PbBr$_4$	(0.28, 0.36)	73	7843	1.39 (λ_{em} = 545 nm; av)	—	34
Cationic 2D lead halide	[Pb2F$_2$][O$_2$C(CH$_2$)$_4$CO$_2$]	(0.33, 0.41)	78	5620	2.64 (λ_{em} = 541 nm; av)	1.8	69
	[Pb2Cl$_2$][O$_2$C(CH$_2$)$_4$CO$_2$]	(0.35, 0.46)	68	5129	2.24 (λ_{em} = 536 nm; av)	11.8	69
	[Pb2Br$_2$][O$_2$C(CH$_2$)$_4$CO$_2$]	(0.42, 0.48)	—	3770	2.25 (λ_{em} = 565 nm; av)	2.0	69
1D nanotube	(HMTA)$_3$Pb$_2$Br$_7$	(0.42, 0.45)	78^a	3572^a	106 (λ_{em} = 580 nm; av)	7%	61
1D perovskite	(DMEDA)PbBr$_4$	(0.21, 0.28)	53	21 242	26–37 (λ_{em} = 475 nm; av)	18–20	60
0D perovskite	(DMEDA)$_4$SnBr$_6$	(0.45, 0.51)^a	54^a	3506^a	2200 (λ_{em} = 570 nm; av)	95	63
	(DMEDA)$_4$SnI$_6$	(0.58, 0.41)^a	71^a	1607^a	1100 (λ_{em} = 620 nm; av)	75	63
	(BMPY)$_2$SbCl$_5$	(0.50, 0.47)^a	61^a	2588^a	4200 (λ_{em} = 590 nm; av)	98	63

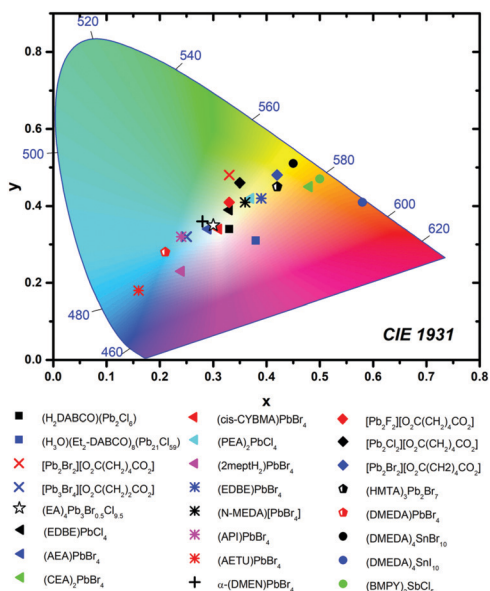^{a} Values calculated from the reported spectra; "av" indicates average lifetimes.

Fig. 7 CIE chromaticity coordinates of broadband emitting metal halide frameworks.

Fig. 8 (a) Distributed Bragg reflector (DBR) coupled to the perovskite (EDBE)PbCl$_4$. PS = polystyrene and CA = cellulose acetate; reprinted with permission from ref. 115 Copyright 2018 American Chemical Society. (b) X-ray excited luminescence of (EDBE)PbCl$_4$; reprinted with permission from ref. 10 Copyright 2016 Springer Nature.

tunability, the ultrabroad PL spectrum of these materials could be modified by engineering their photonic environment so that the PL is suppressed or enhanced in specific spectral regions. In this regard, we have recently shown the directional spectral redistribution of (EDBE)PbCl$_4$ luminescence by incorporation in a polymer microcavity (Fig. 8a).[115] Similarly, perovskite films could be patterned on the sub-wavelength scale (for example through large area techniques like nanoimprint lithography) to enhance the density of photon states leading to Purcell enhancement of luminescence and structural coloring.[116] In the future, these strategies could be applied to allow color tunability in low-cost, flexible LEDs based on a unique broadband emitter without relying on compositional engineering.[115]

Thanks to the solution processability and the presence of heavy atoms which enhance their absorption cross section, hybrid perovskites are also promising for the fabrication of cost-effective, large area X-ray detectors,[117–119] which find application in scientific research as well as in medicine and inspection systems for safety controls. Due to the high exciton binding energy and large Stokes shift, which reduce the negative effect of thermal quenching and the probability of radiation self-absorption, we have shown that X-ray scintillators based on the white-light emitting (EDBE)PbCl$_4$ outperform those based on MAPbI$_3$ and MAPbBr$_3$. In all these perovskites, following X-ray excitation, an afterglow effect extending to thousands of seconds was observed at low temperature (10 K), while showing a negligible contribution at room temperature. The fraction of the total excitation energy accumulated into long-living traps was determined by thermoluminescence measurements, which allows one to compare the luminescence intensity from the end of X-ray excitation until the end of the entire run (I_{TL}), against the luminescence intensity from the beginning of the X-ray excitation to the end of the run ($I_{TL} + I_{ssXL}$). The ratio $I_{TL}/(I_{TL} + I_{ssXL})$ was found to be
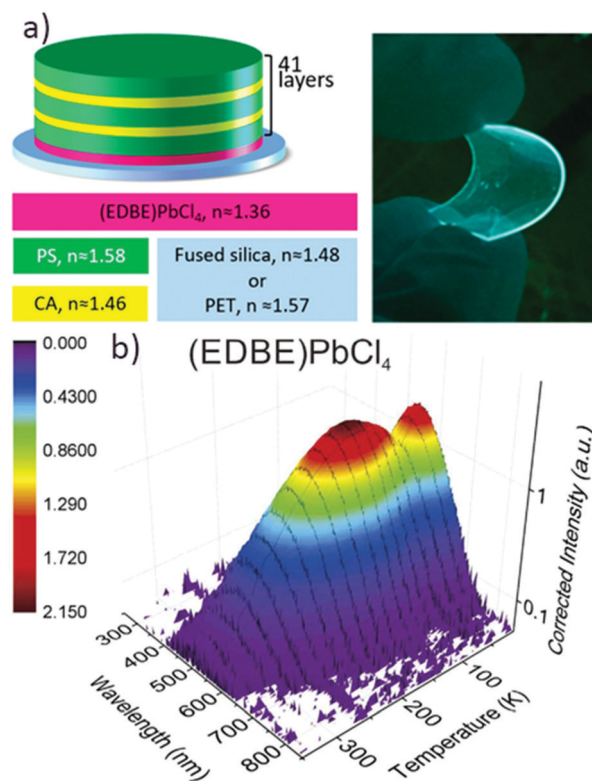
~ 0.002 for the 3D perovskite and ~ 0.058 for (EDBE)PbCl$_4$, which are both low compared to other oxide-based scintillator materials.[10] In particular, higher luminescence yields were achieved in the range 50–298 K (Fig. 8b) with the white emitter (EDBE)PbCl$_4$ as compared to standard 3D perovskites, reaching 9000 photons per MeV at room temperature.[10] Such encouraging performance might be further improved by increasing the luminescence quantum yield of the 2D perovskite through structural design, by doping with lanthanide ions such as Ce^{3+} or by enhancing the X-ray luminescence yield using nanostructured perovskite films (for example via Purcell enhancement).

Beyond the efficient light emitting properties, metal halide perovskites are also emerging due to their attractive gain characteristics,[120–123] which recently allowed the achievement of continuous-wave (c.w.) optically pumped lasing (at $T < 160$ K) in distributed feed-back lasers based on the 3D perovskite MAPbI$_3$.[124] Further improvements are now being achieved with layered perovskites, in particular multidimensional perovskites of the Ruddlesden–Popper series, where energy funneling effects in heterogenous systems allowed low-threshold lasing (13.6 μJ cm^{-2}) and improved gain coefficients (>300 cm^{-1}) to be obtained.[125–127] Such 2D/3D systems can potentially be engineered to obtain an optimal balance between efficient radiative recombination, long radiative lifetime and high carrier mobility,[128] and might hold the key for the realization of long sought-after solution

processed laser diodes.[127] In this context, white light emitting perovskites might offer the attractive possibility to realize tunable lasers across the visible spectral region with a single active material. Nevertheless, the capability to sustain amplified spontaneous emission and lasing in such broadband emitters is yet to be ascertained, urging the need for a deeper understanding of the photophysical processes underlying the broadband luminescence of metal halide lattices.

To further widen the application prospects of broadband emitting perovskites (including, for example, light-emitting field effect transistors and electrically injected lasers),[129] future work will also need to address charge transport and injection issues in these wide band-gap semiconductors as well as elucidate the non-trivial role of small-polaron transport in metal halide frameworks.[130] Indeed, while electroluminescence using narrowband-emitting 2D, multidimensional and 3D perovskites as active materials is now established,[4,5,131,132] direct electrical to optical power conversion in white-light perovskites still remains a challenge.

5 Conclusions

Recent progress in synthetic design suggests that ultrabroadband and highly Stokes shifted luminescence is an intrinsic characteristic of a wide range of metal halide frameworks with low dimensionality. Up to now, the most accredited model to explain this behavior points towards the formation of several self-trapped excitonic species, which can be interpreted as small polarons localized at specific sites of the inorganic lattice. The balance between free and self-trapped excitons is strongly affected by temperature and by the local structural properties of the materials, where stronger deviations from the ideal geometry seem to ease the self-trapping process. While this has been more extensively investigated in 2D perovskites, the analysis of a broader range of low-dimensional structures will be necessary to unequivocally define the common structural properties which stabilize the polaron formation. Several studies are still needed to provide deeper insight into the trapping mechanism, such as electron paramagnetic resonance, neutron diffraction, infrared photoinduced absorption and time resolved photocurrent. These will provide additional information to correlate the structure and optical properties to aid the design of highly efficient white-light emitters for optoelectronic applications, such as light emitting devices and X-ray scintillators.

Conflicts of interest

There are no conflicts to declare.

Acknowledgements

Notes and references

1 M. L. Petrus, J. Schlipf, C. Li, T. P. Gujar, N. Giesbrecht, P. Müller-Buschbaum, M. Thelakkat, T. Bein, S. Hüttner and P. Docampo, *Adv. Energy Mater.*, 2017, **7**, 1700264.

2 B. R. Sutherland and E. H. Sargent, *Nat. Photonics*, 2016, **10**, 295.

3 S. Adjokatse, H.-H. Fang and M. A. Loi, *Mater. Today*, 2017, **20**, 413–424.

4 S. A. Veldhuis, P. P. Boix, N. Yantara, M. Li, T. C. Sum, N. Mathews and S. G. Mhaisalkar, *Adv. Mater.*, 2016, **28**, 6804–6834.

5 M. Yuan, L. N. Quan, R. Comin, G. Walters, R. Sabatini, O. Voznyy, S. Hoogland, Y. Zhao, E. M. Beauregard, P. Kanjanaboos, Z. Lu, D. H. Kim and E. H. Sargent, *Nat. Nano*, 2016, **11**, 872–877.

6 B. Saparov and D. B. Mitzi, *Chem. Rev.*, 2016, **116**, 4558–4596.

7 D. Cortecchia, J. Yin, A. Bruno, S.-Z. A. Lo, G. G. Gurzadyan, S. Mhaisalkar, J.-L. Bredas and C. Soci, *J. Mater. Chem. C*, 2017, **5**, 2771–2780.

8 E. R. Dohner, A. Jaffe, L. R. Bradshaw and H. I. Karunadasa, *J. Am. Chem. Soc.*, 2014, **136**, 13154–13157.

9 H. Tsai, W. Nie, J.-C. Blancon, C. C. Stoumpos, R. Asadpour, B. Harutyunyan, A. J. Neukirch, R. Verduzco, J. J. Crochet, S. Tretiak, L. Pedesseau, J. Even, M. A. Alam, G. Gupta, J. Lou, P. M. Ajayan, M. J. Bedzyk, M. G. Kanatzidis and A. D. Mohite, *Nature*, 2016, **536**, 312.

10 M. D. Birowosuto, D. Cortecchia, W. Drozdowski, K. Brylew, W. Lachmanski, A. Bruno and C. Soci, *Sci. Rep.*, 2016, **6**, 37254.

11 D. B. Mitzi, *Progress in Inorganic Chemistry*, John Wiley & Sons, Inc., 2007, pp. 1–121, DOI: 10.1002/9780470166499.ch1.

12 F. Giustino and H. J. Snaith, *ACS Energy Lett.*, 2016, **1**, 1233–1240.

13 D. Cortecchia, H. A. Dewi, J. Yin, A. Bruno, S. Chen, T. Baikie, P. P. Boix, M. Grätzel, S. Mhaisalkar, C. Soci and N. Mathews, *Inorg. Chem.*, 2016, **55**, 1044–1052.

14 G. Pilania, P. V. Balachandran, C. Kim and T. Lookman, *Front. Mater.*, 2016, **3**, 19.

15 D. B. Mitzi, *Functional Hybrid Materials*, Wiley-VCH Verlag GmbH & Co. KGaA, 2005, pp. 347–386, DOI: 10.1002/3527602372.ch10.

16 Z. Cheng and J. Lin, *CrystEngComm*, 2010, **12**, 2646–2662.

17 D. B. Mitzi, *J. Chem. Soc., Dalton Trans.*, 2001, 1–12, DOI: 10.1039/B007070J.

18 D. B. Mitzi, *J. Solid State Chem.*, 1999, **145**, 694–704.

19 C. C. Stoumpos, D. H. Cao, D. J. Clark, J. Young, J. M. Rondinelli, J. I. Jang, J. T. Hupp and M. G. Kanatzidis, *Chem. Mater.*, 2016, **28**, 2852–2867.

20 D. B. Mitzi, K. Liang and S. Wang, *Inorg. Chem.*, 1998, **37**, 321–327.

21 Y. Y. Li, C. K. Lin, G. L. Zheng, Z. Y. Cheng, H. You, W. D. Wang and J. Lin, *Chem. Mater.*, 2006, **18**, 3463–3469.

22 J. Zaleski and A. Pietraszko, *Acta Crystallogr., Sect. B: Struct. Sci.*, 1996, **52**, 287–295.

23 A. Kallel and J. W. Bats, *Acta Crystallogr., Sect. C: Cryst. Struct. Commun.*, 1985, **41**, 1022–1024.

24 D. Cortecchia, K. C. Lew, J.-K. So, A. Bruno and C. Soci, *Chem. Mater.*, 2017, **29**, 10088–10094.

25 M. E. Kamminga, G. A. de Wijs, R. W. A. Havenith, G. R. Blake and T. T. M. Palstra, *Inorg. Chem.*, 2017, **56**, 8408–8414.

26 J. L. Knutson, J. D. Martin and D. B. Mitzi, *Inorg. Chem.*, 2005, **44**, 4699–4705.

27 K.-z. Du, Q. Tu, X. Zhang, Q. Han, J. Liu, S. Zauscher and D. B. Mitzi, *Inorg. Chem.*, 2017, **56**, 9291–9302.

28 S. Meloni, G. Palermo, N. Ashari-Astani, M. Gratzel and U. Rothlisberger, *J. Mater. Chem. A*, 2016, **4**, 15997–16002.

29 R. Prasanna, A. Gold-Parker, T. Leijtens, B. Conings, A. Babayigit, H.-G. Boyen, M. F. Toney and M. D. McGehee, *J. Am. Chem. Soc.*, 2017, **139**, 11117–11124.

30 N. Kawano, M. Koshimizu, Y. Sun, N. Yahaba, Y. Fujimoto, T. Yanagida and K. Asai, *J. Phys. Chem. C*, 2014, **118**, 9101–9106.

31 K. Robinson, G. V. Gibbs and P. H. Ribbe, *Science*, 1971, **172**, 567–570.

32 I. Neogi, A. Bruno, D. Bahulayan, T. W. Goh, B. Ghosh, R. Ganguly, D. Cortecchia, T. C. Sum, C. Soci, N. Mathews and S. G. Mhaisalkar, *ChemSusChem*, 2017, **10**, 3765–3772.

33 L. Mao, Y. Wu, C. C. Stoumpos, B. Traore, C. Katan, J. Even, M. R. Wasielewski and M. G. Kanatzidis, *J. Am. Chem. Soc.*, 2017, **139**, 11956–11963.

34 L. Mao, Y. Wu, C. C. Stoumpos, M. R. Wasielewski and M. G. Kanatzidis, *J. Am. Chem. Soc.*, 2017, **139**, 5210–5215.

35 D. Cortecchia, S. Neutzner, A. R. Srimath Kandada, E. Mosconi, D. Meggiolaro, F. De Angelis, C. Soci and A. Petrozza, *J. Am. Chem. Soc.*, 2017, **139**, 39–42.

36 D. Cortecchia, S. Neutzner, J. Yin, T. Salim, A. R. S. Kandada, A. Bruno, Y. M. Lam, J. Martí-Rujas, A. Petrozza and C. Soci, *APL Mater.*, 2018, **6**, 114207.

37 J. A. Alonso, M. J. Martínez-Lope, M. T. Casais and M. T. Fernández-Díaz, *Inorg. Chem.*, 2000, **39**, 917–923.

38 M. E. Kamminga, H.-H. Fang, M. R. Filip, F. Giustino, J. Baas, G. R. Blake, M. A. Loi and T. T. M. Palstra, *Chem. Mater.*, 2016, **28**, 4554–4562.

39 T. Kenichiro, T. Takayuki, K. Takashi, U. Kenichi, E. Kazuhiro, U. Tsutomu, A. Keisuke, U. Kazuhito and M. Noboru, *Jpn. J. Appl. Phys.*, 2005, **44**, 5923.

40 T. Ishihara, *Optical Properties of Low–Dimensional Materials*, 1996, pp. 288–339, DOI: 10.1142/9789814261388_0006.

41 X. Wu, M. T. Trinh and X. Y. Zhu, *J. Phys. Chem. C*, 2015, **119**, 14714–14721.

42 K. Galkowski, A. Mitioglu, A. Miyata, P. Plochocka, O. Portugall, G. E. Eperon, J. T.-W. Wang, T. Stergiopoulos, S. D. Stranks, H. J. Snaith and R. J. Nicholas, *Energy Environ. Sci.*, 2016, **9**, 962–970.

43 V. D'Innocenzo, G. Grancini, M. J. P. Alcocer, A. R. S. Kandada, S. D. Stranks, M. M. Lee, G. Lanzani, H. J. Snaith and A. Petrozza, *Nat. Commun.*, 2014, **5**, 3586.

44 S. Gonzalez-Carrero, G. M. Espallargas, R. E. Galian and J. Perez-Prieto, *J. Mater. Chem. A*, 2015, **3**, 14039–14045.

45 F. Thouin, S. Neutzner, D. Cortecchia, V. A. Dragomir, C. Soci, T. Salim, Y. M. Lam, R. Leonelli, A. Petrozza, A. R. S. Kandada and C. Silva, *Phys. Rev. Mater.*, 2018, **2**, 034001.

46 H. Lin, C. Zhou, Y. Tian, T. Siegrist and B. Ma, *ACS Energy Lett.*, 2018, **3**, 54–62.

47 M. D. Smith and H. I. Karunadasa, *Acc. Chem. Res.*, 2018, **51**, 619–627.

48 J. Yin, H. Li, D. Cortecchia, C. Soci and J.-L. Brédas, *ACS Energy Lett.*, 2017, **2**, 417–423.

49 A. Yangui, S. Pillet, E.-E. Bendeif, A. Lusson, S. Triki, Y. Abid and K. Boukheddaden, *ACS Photonics*, 2018, **5**, 1599–1611.

50 S. Wang, Y. Yao, J. Kong, S. Zhao, Z. Sun, Z. Wu, L. Li and J. Luo, *Chem. Commun.*, 2018, **54**, 4053–4056.

51 T. Hu, M. D. Smith, E. R. Dohner, M.-J. Sher, X. Wu, M. T. Trinh, A. Fisher, J. Corbett, X. Y. Zhu, H. I. Karunadasa and A. M. Lindenberg, *J. Phys. Chem. Lett.*, 2016, **7**, 2258–2263.

52 A. Yangui, D. Garrot, J. S. Lauret, A. Lusson, G. Bouchez, E. Deleporte, S. Pillet, E. E. Bendeif, M. Castro, S. Triki, Y. Abid and K. Boukheddaden, *J. Phys. Chem. C*, 2015, **119**, 23638–23647.

53 M. D. Smith, A. Jaffe, E. R. Dohner, A. M. Lindenberg and H. I. Karunadasa, *Chem. Sci.*, 2017, **8**, 4497–4504.

54 Y. Li, G. Zheng and J. Lin, *Eur. J. Inorg. Chem.*, 2008, 1689–1692.

55 E. R. Dohner, E. T. Hoke and H. I. Karunadasa, *J. Am. Chem. Soc.*, 2014, **136**, 1718–1721.

56 E. P. Booker, T. H. Thomas, C. Quarti, M. R. Stanton, C. D. Dashwood, A. J. Gillett, J. M. Richter, A. J. Pearson, N. J. L. K. Davis, H. Sirringhaus, M. B. Price, N. C. Greenham, D. Beljonne, S. E. Dutton and F. Deschler, *J. Am. Chem. Soc.*, 2017, **139**, 18632–18639.

57 Y. N. Ivanov, A. A. Sukhovskii, V. V. Lisin and I. P. Aleksandrova, *Inorg. Mater.*, 2001, **37**, 623–627.

58 C. Jen-Hui, D. Thomas and R. Michael, *Z. Anorg. Allg. Chem.*, 2016, **642**, 736–748.

59 K. M. McCall, C. C. Stoumpos, S. S. Kostina, M. G. Kanatzidis and B. W. Wessels, *Chem. Mater.*, 2017, **29**, 4129–4145.

60 Z. Yuan, C. Zhou, Y. Tian, Y. Shu, J. Messier, J. C. Wang, L. J. van de Burgt, K. Kountouriotis, Y. Xin, E. Holt, K. Schanze, R. Clark, T. Siegrist and B. Ma, *Nat. Commun.*, 2017, **8**, 14051.

61 H. Lin, C. Zhou, Y. Tian, T. Besara, J. Neu, T. Siegrist, Y. Zhou, J. Bullock, K. S. Schanze, W. Ming, M.-H. Du and B. Ma, *Chem. Sci.*, 2017, **8**, 8400–8404.

62 G. Wu, C. Zhou, W. Ming, D. Han, S. Chen, D. Yang, T. Besara, J. Neu, T. Siegrist, M.-H. Du, B. Ma and A. Dong, *ACS Energy Lett.*, 2018, **3**, 1443–1449.

63 C. Zhou, H. Lin, Y. Tian, Z. Yuan, R. Clark, B. Chen, L. J. van de Burgt, J. C. Wang, Y. Zhou, K. Hanson, Q. J. Meisner, J. Neu, T. Besara, T. Siegrist, E. Lambers, P. Djurovich and B. Ma, *Chem. Sci.*, 2018, **9**, 586–593.

64 J. Luo, X. Wang, S. Li, J. Liu, Y. Guo, G. Niu, L. Yao, Y. Fu, L. Gao, Q. Dong, C. Zhao, M. Leng, F. Ma, W. Liang,

This journal is © The Royal Society of Chemistry 2019

J. Mater. Chem. C, 2019, **7**, 4956–4969 | 4967

L. Wang, S. Jin, J. Han, L. Zhang, J. Etheridge, J. Wang, Y. Yan, E. H. Sargent and J. Tang, *Nature*, 2018, **563**, 541–545.

65 X. Wang, W. Meng, W. Liao, J. Wang, R.-G. Xiong and Y. Yan, *J. Phys. Chem. Lett.*, 2019, **10**, 501–506.

66 S. Krishnamurthy, R. Naphade, W. J. Mir, S. Gosavi, S. Chakraborty, R. Vaidhyanathan and S. Ogale, *Adv. Opt. Mater.*, 2018, **6**, 1800751.

67 M. D. Smith, B. L. Watson, R. H. Dauskardt and H. I. Karunadasa, *Chem. Mater.*, 2017, **29**, 7083–7087.

68 G.-E. Wang, G. Xu, M.-S. Wang, L.-Z. Cai, W.-H. Li and G.-C. Guo, *Chem. Sci.*, 2015, **6**, 7222–7226.

69 Z. Zhuang, C. Peng, G. Zhang, H. Yang, J. Yin and H. Fei, *Angew. Chem., Int. Ed.*, 2017, **56**, 14411–14416.

70 C. Peng, Z. Zhuang, H. Yang, G. Zhang and H. Fei, *Chem. Sci.*, 2018, **9**, 1627–1633.

71 R. T. Williams and K. S. Song, *J. Phys. Chem. Solids*, 1990, **51**, 679–716.

72 K. Thirumal, W. K. Chong, W. Xie, R. Ganguly, S. K. Muduli, M. Sherburne, M. Asta, S. Mhaisalkar, T. C. Sum, H. S. Soo and N. Mathews, *Chem. Mater.*, 2017, **29**, 3947–3953.

73 I. Pelant and J. Valenta, *Luminescence Spectroscopy of Semiconductors*, OUP, Oxford, 2012.

74 X. Y. Zhu and V. Podzorov, *J. Phys. Chem. Lett.*, 2015, **6**, 4758–4761.

75 R. P. Feynman, *Phys. Rev.*, 1955, **97**, 660–665.

76 H. Fröhlich, *Adv. Phys.*, 1954, **3**, 325–361.

77 J. Ma and L. W. Wang, *Nano Lett.*, 2015, **15**, 248–253.

78 K. Miyata, D. Meggiolaro, M. T. Trinh, P. P. Joshi, E. Mosconi, S. C. Jones, F. De Angelis and X. Y. Zhu, *Sci. Adv.*, 2017, **3**, e1701217.

79 W. P. D. Wong, J. Yin, B. Chaudhari, C. Xin Yu, D. Cortecchia, S.-Z. A. Lo, C. A. Grimsdale, G. Lanzani and C. Soci, to be submitted.

80 D. Emin, *Phys. Rev. B: Condens. Matter Mater. Phys.*, 1993, **48**, 13691–13702.

81 T. Ivanovska, C. Dionigi, E. Mosconi, F. De Angelis, F. Liscio, V. Morandi and G. Ruani, *J. Phys. Chem. Lett.*, 2017, **8**, 3081–3086.

82 H. M. Zhu, K. Miyata, Y. P. Fu, J. Wang, P. P. Joshi, D. Niesner, K. W. Williams, S. Jin and X. Y. Zhu, *Science*, 2016, **353**, 1409–1413.

83 G. Batignani, G. Fumero, A. R. Srimath Kandada, G. Cerullo, M. Gandini, C. Ferrante, A. Petrozza and T. Scopigno, *Nat. Commun.*, 2018, **9**, 1971.

84 M. Park, A. J. Neukirch, S. E. Reyes-Lillo, M. Lai, S. R. Ellis, D. Dietze, J. B. Neaton, P. Yang, S. Tretiak and R. A. Mathies, *Nat. Commun.*, 2018, **9**, 2525.

85 J. Yin, Y. Zhang, A. Bruno, C. Soci, O. M. Bakr, J.-L. Brédas and O. F. Mohammed, *ACS Energy Lett.*, 2017, **2**, 2805–2811.

86 J. Yin, P. Maity, M. De Bastiani, I. Dursun, O. M. Bakr, J.-L. Brédas and O. F. Mohammed, *Sci. Adv.*, 2017, **3**, e1701793.

87 S. Neutzner, F. Thouin, D. Cortecchia, A. Petrozza, C. Silva and A. R. Srimath Kandada, *Phys. Rev. Mater.*, 2018, **2**, 064605.

88 F. Thouin, D. A. Valverde-Chávez, C. Quarti, D. Cortecchia, I. Bargigia, D. Beljonne, A. Petrozza, C. Silva and A. R. Srimath Kandada, *Nat. Mater.*, 2019, **18**, 349–356.

89 D. Emin, *Polarons*, Cambridge University Press, 2013.

90 J. G. Mance, J. J. Felver and S. L. Dexheimer, *J. Phys. Chem. C*, 2014, **118**, 11186–11192.

91 W. Känzig, *J. Phys. Chem. Solids*, 1960, **17**, 88–92.

92 C.-t. Kao, L. G. Rowan and L. M. Slifkin, *Phys. Rev. B: Condens. Matter Mater. Phys.*, 1990, **42**, 3142–3151.

93 S. V. Nistor and D. Schoemaker, *Phys. Status Solidi B*, 1995, **190**, 339–346.

94 S. V. Nistor, E. Goovaerts and D. Schoemaker, *Phys. Rev. B: Condens. Matter Mater. Phys.*, 1993, **48**, 9575–9580.

95 M. Iwanaga, J. Azuma, M. Shirai, K. Tanaka and T. Hayashi, *Phys. Rev. B: Condens. Matter Mater. Phys.*, 2002, **65**, 214306.

96 B. Kang and K. Biswas, *J. Phys. Chem. C*, 2016, **120**, 12187–12195.

97 A. M. Stoneham, J. Gavartin, A. L. Shluger, A. V. Kimmel, D. M. Ramo, H. M. Rønnow, G. Aeppli and C. Renner, *J. Phys.: Condens. Matter*, 2007, **19**, 255208.

98 A. M. Stoneham, *Theory of Defects in Solids: Electronic Structure of Defects in Insulators and Semiconductors*, Clarendon Press, 2001.

99 J. L. Gavartin, D. M. Ramo, A. L. Shluger, G. Bersuker and B. H. Lee, *Appl. Phys. Lett.*, 2006, **89**, 082908.

100 D. L. Griscom, *J. Non-Cryst. Solids*, 2006, **352**, 2601–2617.

101 O. F. Schirmer, P. Koidl and H. G. Reik, *Phys. Status Solidi B*, 1974, **62**, 385–391.

102 F. De Angelis and A. Petrozza, *Nat. Mater.*, 2018, **17**, 383–384.

103 D. Meggiolaro, S. G. Motti, E. Mosconi, A. J. Barker, J. Ball, C. Andrea Riccardo Perini, F. Deschler, A. Petrozza and F. De Angelis, *Energy Environ. Sci.*, 2018, **11**, 702–713.

104 C. C. Boyd, R. Cheacharoen, T. Leijtens and M. D. McGehee, *Chem. Rev.*, 2019, **119**, 3418–3451.

105 M. D. Smith, E. J. Crace, A. Jaffe and H. I. Karunadasa, *Annu. Rev. Mater. Res.*, 2018, **48**, 111–136.

106 G. M. Paternò, N. Mishra, A. J. Barker, Z. Dang, G. Lanzani, L. Manna and A. Petrozza, *Adv. Funct. Mater.*, 2018, 1805299.

107 E. E. Rodriguez, T. Proffen, A. Llobet, J. J. Rhyne and J. F. Mitchell, *Phys. Rev. B: Condens. Matter Mater. Phys.*, 2005, **71**, 104430.

108 H. M. Rønnow, C. Renner, G. Aeppli, T. Kimura and Y. Tokura, *Nature*, 2006, **440**, 1025.

109 Z. Wang, J. Zhao, B. Frank, Q. Ran, G. Adamo, H. Giessen and C. Soci, *Nano Lett.*, 2015, **15**, 5382–5387.

110 A. Troisi, *Chem. Soc. Rev.*, 2011, **40**, 2347–2358.

111 M. H. Crawford, *IEEE J. Sel. Top. Quantum Electron.*, 2009, **15**, 1028–1040.

112 E. F. Schubert and J. K. Kim, *Science*, 2005, **308**, 1274–1278.

113 S. Pimputkar, J. S. Speck, S. P. DenBaars and S. Nakamura, *Nat. Photonics*, 2009, **3**, 180–182.

114 Z. Yuan, C. Zhou, J. Messier, Y. Tian, Y. Shu, J. Wang, Y. Xin and B. Ma, *Adv. Opt. Mater.*, 2016, **4**, 2009–2015.

4968 | *J. Mater. Chem. C*, 2019, **7**, 4956–4969

This journal is © The Royal Society of Chemistry 2019

115 P. Lova, D. Cortecchia, H. N. S. Krishnamoorthy, P. Giusto, C. Bastianini, A. Bruno, D. Comoretto and C. Soci, *ACS Photonics*, 2018, **5**, 867–874.

116 B. Gholipour, G. Adamo, D. Cortecchia, H. N. S. Krishnamoorthy, M. D. Birowosuto, N. I. Zheludev and C. Soci, *Adv. Mater.*, 2017, **29**, 1604268.

117 H. Wei, Y. Fang, P. Mulligan, W. Chuirazzi, H.-H. Fang, C. Wang, B. R. Ecker, Y. Gao, M. A. Loi, L. Cao and J. Huang, *Nat. Photonics*, 2016, **10**, 333–339.

118 S. Yakunin, M. Sytnyk, D. Kriegner, S. Shrestha, M. Richter, G. J. Matt, H. Azimi, C. J. Brabec, J. Stangl, M. V. Kovalenko and W. Heiss, *Nat. Photonics*, 2015, **9**, 444–449.

119 S. Yakunin, D. N. Dirin, Y. Shynkarenko, V. Morad, I. Cherniukh, O. Nazarenko, D. Kreil, T. Nauser and M. V. Kovalenko, *Nat. Photonics*, 2016, **10**, 585–589.

120 P. J. Cegielski, S. Neutzner, C. Porschatis, H. Lerch, J. Bolten, S. Suckow, A. R. S. Kandada, B. Chmielak, A. Petrozza, T. Wahlbrink and A. L. Giesecke, *Opt. Express*, 2017, **25**, 13199–13206.

121 F. Deschler, M. Price, S. Pathak, L. E. Klintberg, D.-D. Jarausch, R. Higler, S. Hüttner, T. Leijtens, S. D. Stranks, H. J. Snaith, M. Atatüre, R. T. Phillips and R. H. Friend, *J. Phys. Chem. Lett.*, 2014, **5**, 1421–1426.

122 S. Neutzner, A. R. Srimath Kandada, G. Lanzani and A. Petrozza, *J. Mater. Chem. C*, 2016, **4**, 4630–4633.

123 G. Xing, N. Mathews, S. S. Lim, N. Yantara, X. Liu, D. Sabba, M. Grätzel, S. Mhaisalkar and T. C. Sum, *Nat. Mater.*, 2014, **13**, 476.

124 Y. Jia, R. A. Kerner, A. J. Grede, B. P. Rand and N. C. Giebink, *Nat. Photonics*, 2017, **11**, 784–788.

125 C. M. Raghavan, T.-P. Chen, S.-S. Li, W.-L. Chen, C.-Y. Lo, Y.-M. Liao, G. Haider, C.-C. Lin, C.-C. Chen, R. Sankar, Y.-M. Chang, F.-C. Chou and C.-W. Chen, *Nano Lett.*, 2018, **18**, 3221–3228.

126 Z. Haihua, L. Qing, W. Yishi, Z. Zhaoyi, G. Qinggang, L. Peng, L. Meili, Y. Jiannian and F. Hongbing, *Adv. Mater.*, 2018, **30**, 1706186.

127 L. Meili, G. Qinggang, L. Peng, L. Qing, Z. Haihua, Y. Jiannian, H. Wenping, W. Yishi and F. Hongbing, *Adv. Funct. Mater.*, 2018, **28**, 1707006.

128 G. Xing, B. Wu, X. Wu, M. Li, B. Du, Q. Wei, J. Guo, E. K. L. Yeow, T. C. Sum and W. Huang, *Nat. Commun.*, 2017, **8**, 14558.

129 X. Y. Chin, D. Cortecchia, J. Yin, A. Bruno and C. Soci, *Nat. Commun.*, 2015, **6**, 7383.

130 A. J. E. Rettie, W. D. Chemelewski, D. Emin and C. B. Mullins, *J. Phys. Chem. Lett.*, 2016, **7**, 471–479.

131 D. Liang, Y. Peng, Y. Fu, M. J. Shearer, J. Zhang, J. Zhai, Y. Zhang, R. J. Hamers, T. L. Andrew and S. Jin, *ACS Nano*, 2016, **10**, 6897–6904.

132 M. Era, S. Morimoto, T. Tsutsui and S. Saito, *Appl. Phys. Lett.*, 1994, **65**, 676–678.